ChemComm

Accepted Manuscript

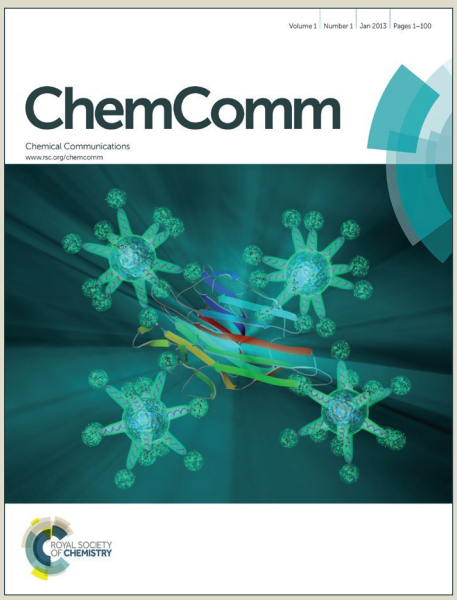

ROYAL SOCIETY OF CHEMISTRY

www.rsc.org/chemcomm

ChemComm

RSCPublishing

COMMUNICATION

Fabrication of three dimensional (3D) hierarchical Ag/WO_3 flower-like catalyst materials for the selective oxidation of *m*-xylene to isophthalic acid

Cite this: DOI: 10.1039/x0xx00000x

Received ooth January 2012,
Accepted ooth January 2012

DOI: 10.1039/x0xx00000x

www.rsc.org/

Shankha S. Acharyya,[a] Shilpi Ghosh,[a] and Rajaram Bal*[a]

Three dimensional (3D) hierarchical silver supported tungsten oxide flower-like microspheres catalyst have been fabricated by a cationic surfactant CTAB. It was found that crystal-splitting mechanism plays a key role in the formation of this flower-like structure. This catalyst was proved to be highly effective in liquid phase selective oxidation of *m*-xylene to isophthalic acid.

Design of highly ordered superstructures with tunable morphologies and structure assembled by low-dimensional inorganic nanostructures is of potential interest in material chemistry owing to their novel properties and fundamental importance in various application fields.[1] Recently, extensive researches have been devoted in the investigation of efficient methodologies to synthesize functional materials with complex three-dimensional (3D) nanostructures[2] such as Fe flower-like spheres with better adsorption performance on water treatment,[3] cactus-like β-Ga_2O_3 nanostructures with good field emission activity,[4] hollow Fe_3O_4 spheres with excellent super-paramagnetic character,[5] hollow V_2O_5 spheres with high capacity and remarkable reversibility in lithium batteries,[6] flower-like β-In_2S_3 with ultra high specific surface area,[7] hierarchical pompon-like Co_3O_4 porous spheres for high-performance lithium-ion batteries etc.[8] Moreover, the large cavities of the 3D frameworks can alleviate volume strain and stabilize the structures during the intercalation-deintercalation processes.[8] However, the controlled construction of 3D architectures from nanobuilding blocks via chemical routes still remains a challenge in material chemistry research because control of the nucleation and growth of nanomaterials is really a mammoth task.[7,9] The simplest synthetic route to 3D nanostructures is the self-assembly, in which ordered aggregates are formed in a spontaneous process and thus the process has become an important technique to execute fabrication of sophisticated architechtures.[1e,2] However, the development of simple and reliable synthetic methods for hierarchically self-assembled architectures with designed chemical components and tunable morphologies still remains a challenge for the researchers. Very recently, our group reported fabrication of three-dimensional (3D) raspberry-like copper chromite spinel catalyst in hydrothermal route, for the selective oxidation of benzene to phenol with high yield.[10] Being inspired by our own reports, we tried to tune up similar morphology in case of Ag-W nanostructures. In the path of our research, we reported various morphologies of Ag-W nanostructures.[11] Herein, we report the novel three-dimensional Ag/WO_3 hierarchical flower-like microspheres assembled by nanopetals, which has seldom been reported.

The commercial application of isophthalic acid (IPA) and terephthalic acid as chemical materials is becoming more and more broadly.[12] These aromatic dicarboxylic acids are used as precursors (in form of acyl chlorides) to commercially important polymers, e.g. the fire-resistant material Nomex. Mixed with terephthalic acid, IPA is used in the production of resins for drink bottles. The high-performance polymer polybenzimidazole is produced from IPA. IPA is produced on the billion kg per year scale by oxidizing *m*-xylene using oxygen by conventional Amoco Oxidation process involving homogeneous Co–Mn–Br catalyst system in acetic acid medium.[12] This process suffers not only from low yield, but involves the use of bromine, which is corrosive, that erodes the expensive reactors. Moreover, undesirable methyl bromide is produced from the reaction system is added to the atmosphere, that can deplete the ozone layer. Furthermore, since the reaction is highly exothermic much of the reactant molecules (*m*-xylene) are released from the reaction system.[12] Ishii et al.[13] have developed an efficient bromide-free catalyst package which combines $Co(OAc)_2$ and N-hydroxyphthalimide to oxidize *p*-xylene to terephthalic acid. Saha obtained acceptable rates and yields of terephthalic by using N-hydroxyphthalimide (NHPI) and its derivatives,[14] such as 3F–NHPI, 4-Me–NHPI and N-acetoxyphthalimide, as promoters with $Co(OAc)_2$ catalyst for the autoxidation of *p*-xylene and other methyl arenes. Wentzel et al.[15] reported the Co^{2+}/NHPI-catalyzed

autoxidation of ethylbenzene. They suggested that 3-F–NHPI is most active, particularly at the initial stage of the reaction. Thereafter, Long and his group[16] reported a bromine-free catalyst system consisting of $H_3PW_{12}O_{40}$ (HPW)/$Co(OAc)_2$/$Mn(OAc)_2$ and HPW/coconut activated carbon and Co-catalytic system to oxidize *m*-xylene using molecular oxygen as oxidant at 220 °C. Lee and his group reported formation of IPA (with isolated yield 30%) under microwave irradiation (130 °C) using TBHP as oxidant.[17] Very recently, Deka and his group reported liquid phase oxidation of *p*-xylene to terephthalic acid (with >99% yield) at 70°C at 24 h using oxygen as oxidant.[18] But, so far, there is no literature that report of furnishing IPA from *m*-xylene with high yield. Herein, we report *m*-xylene conversion of >99% with an IPA selectivity of 97% using our so-prepared three-dimensional Ag/WO_3 hierarchical flower-like catalyst at 70 °C, with H_2O_2 as oxidant.

The Ag/WO_3 flower-like nanocomposite was synthesized modifying our own preparation method using nitrite precursors of Ag,[11] and was characterized by XRD, XPS, SEM, TEM, Raman, FTIR, TGA, BET surface area and ICP-AES. The X-ray diffraction (XRD) pattern of the Ag-W catalyst showed the peaks at 2θ values of 23.1º, 23.7º, 24.4º, 33.3º and 34.0º, confirm the formation of monoclinic WO_3 (JCPDS No. 43-1035, space group: P21/n) (Fig.1). However, we could not observe any diffraction peaks assignable to metallic silver Ag (0) or oxides of silver, indicating the very small silver particles size. X-ray photoelectron spectroscopy (XPS) analyses confirmed the presence of metallic silver in the fresh sample from the corresponding Ag $3d_{5/2}$ and Ag $3d_{3/2}$ binding energy values of 368.2 eV and 374.2 eV respectively (Fig. S1, ESI†).[11] The W $4f_{5/2}$ and $4f_{7/2}$ spectra attributed to the binding energies 37.9 eV and 35.8 eV respectively suggesting that the tungsten in the tungsten oxide sample exists as W^{+6}.[11,19] (Fig. S2, ESI†). The corresponding Ag 3d binding energy of the spent catalyst ~368.3 eV, confirms that the oxidation state of metallic silver does not change during catalysis. (Fig. S1b, ESI†). Raman spectra of the Ag/WO_3 flower catalyst is characterized by well resolved sharp bands as shown in Fig. S3, ESI†. The two main intense peaks at 806 and 718 cm^{-1}, and the shoulder at 686 cm^{-1}, are typical Raman peaks of crystalline WO_3, which correspond to the stretching and bending vibrations of the bridging tungsten and oxygen atoms.[20] They are assigned to be the W–O stretching (υ), W–O bending (δ) and O–W–O deformation (γ) modes, respectively. Two peaks at 326 and 274 cm^{-1} are assigned to be the bending δ(O–W–O) vibrations.[21] Those below 200 cm^{-1} modes were attributed to the lattice vibrations.[21] After the reaction, the Raman spectrum of the spent catalyst was unchanged, reflects the structural stability of the catalyst under the reaction condition. The shape and morphology of the product have been investigated using the SEM (Fig 2). SEM images with lower magnifications revealed that the catalyst comprises several microspheres (30-50 μm diameters). However, higher magnification (Fig 2d,e) displayed that each microsphere is composed of several thousands of divergent swords like petals having sharp tiny tips projecting outwardly with comparable lengths having a common wider base and which thus form a spherical flower-like assembly with a diameter of 30-50 μm. The typical length of one petal is identified as 700–800 nm, while the widths of the bases and tips are in the range of 50–30 nm and 5–10 nm respectively. The SEM elemental mapping indicates the presence of Ag, W and O species and further ascertains the uniformly dispersion of AgNPs on WO_3 support (Fig 2g). TEM measurements were carried out to check the particle size and distribution of the silver nanoparticles (Fig 3, S4, ESI†). HRTEM revealed that the catalyst is composed of highly dispersed very small silver nanoparticles of ~2-5 nm on WO_3 support (Fig. 3a). The corresponding TEM histogram of Ag nanoparticles showed a very narrow particle size distribution with sizes between 2.5-6.5 nm (Fig. S4b, ESI†). The interplanar spacing of the lattice fringe distance of 0.38 nm indicates the [020] lattice spacing of WO_3, which was clearly discriminated from of 0.23 nm corresponds to [111] plane of Ag (Fig. 3b). SAED pattern (Fig. S5, ESI†) exhibited the inter planar spacing distances of 0.20 nm and 0.14 nm, these are indexed to Ag (200) and (220) respectively, which refer to the unique characteristic of the fcc structure of Ag. In addition, the SAED pattern also displayed a polycrystalline nature of the hierarchical structure, indicating that the nano-petals of the AgW flowers are randomly orientated. Furthermore, the TEM image of the spent catalyst showed that the topology and the silver particle size of the catalyst were hardly changed after four reuses (Fig S4c & d, ESI†). TEM-EDX pattern also showed the presence of Ag and W in the sample (Fig. S6, ESI†). Moreover, that the percentage of Ag and W remain intact after four reuses qualitatively is also visualized from the corresponding TEM-EDAX image of the spent catalyst (Fig. S7, ESI†).

The formation of three dimensional (3D) silver supported tungsten oxide flower-like microspheres catalyst is really interesting although the mechanism is not very clear. To explore the formation mechanism of 3D self-assembled flower-like $Ag-WO_3$ microspheres, a series of time-dependent experiments were performed. In the absence of CTAB, disperse rods with indefinite aspect ratio were obtained (Fig. S8, ESI†). However, inhomogenous flower-like nanostructures with small diameters assembled by disordered nanopetals were obtained while Ag: CTAB molar ratio was 1: 0.3 (Fig. S9, ESI†). This experimental finding refelected the structure-directive property of CTAB. Only aggregates of nanoparticles could be observed initially (Fig. S10, ESI†); With stirring time, the nanoparticles assemble under template effect to form petal-like structure (Fig. S11, ESI†). However, several nanopetals, whose orientations gradually deviate from that of the initial crystal, fused together by means of Ostwald ripening and thus, flower-like microspheres start growing; this phenomenon indicated the fact that, these microspheres formed by crystal-splitting growth mechanism.[8] While the stirring time was prolonged to 12 h, non-uniform plate-like structures became the predominant (Fig. S12, ESI†). CTAB molecules in solution act as "soft template" and facilitates self-assembly-mechanism. As a cationic surfactant, CTAB is an ionic compound that ionized completely in water: quantities of anions OH^-, WO_4^{2-}, and Ag and cations CTA^+, Ag^+ existed in basic solution.[21] Therefore, cooperative self-assembly between ionic CTAB molecules and charged species is built via electrostatic interaction in reaction solution. The formation of nearly spherical aggregates of nanoparticles after 3h stirring may be brought from the strong electrostatic attraction between positive CTA^+ cations and negative OH^- anions on the surface of nanoparticles as well as the hydrophobic interactions and van der Waals attraction caused by adjacent CTAB adsorbing on $Ag-WO_3$ nanoparticles. Although there was an intrinsic tendency for nucleation growth along the 1D direction of $Ag-WO_3$ nanoparticles in basic medium,[11c] nano-petal formation is mediated not only by CTAB, but also use of nitrite precursor of silver ($AgNO_2$)(as confirmed from SEM images using different precursors of Ag and W, Fig S13-S15, ESI†). The presence of embedded CTAB-moieties in the uncalcined catalyst can be inferred from the FTIR spectra (Fig. S16, ESI†). The characteristic peaks of CTAB disappeared in FTIR spectra of sample after calcination, in accord with TGA analysis results (Fig. S17, ESI†).

The activity of the catalyst (designated as AgW^{flw}) in selective oxidation of *m*-xylene has been shown in Table 1. We noticed that, temperature played a crucial role in the oxidation reaction of *m*-

xylene (Fig. S20, ESI†). At RT, although appreciable conversion of *m*-xylene was noticed, but, selectivity was very poor. Increment in temperature increased the selectivity, as well as yield of IPA), and the maximum yield (96%), with highest selectivity to IPA (97%) was achieved at 70 °C. But above 70 °C, yield of IPA decreased rapidly due to the formation of benzoic acid, formic acid etc. We also noticed that, optimum molar ratio of *m*-xylene : H_2O_2 was 1:6; probably, excess H_2O_2 was needed, since major amount of H_2O_2 decomposed over the catalyst at the reaction temperature. When of *m*-xylene : H_2O_2 was 1:1 or 1:3, m-tolualdehyde (3-IMA), m-toluic acid (MTA) and 3-carboxybenzaldehyde (3-CBA) were detected in major amount compared to IPA. (Fig. S22, ESI†). When *m*-xylene : H_2O_2 was 1:10, we observed the quick formation of IPA with high yield (~99%) with 4h reaction time, but then the selectivity went decreasing due to the formation of benzaldehyde, benzoic acid and 3-hydroxy-isophthalic acid. The oxidation of *m*-xylene was also dependent on the amount of catalyst used. No IPA was detected in absence of any catalyst (Entry 1, Table 1); increment of catalyst weight, yield of IPA was increased, probably due to the increment of active Ag-sites. Further increment of catalyst weight (>0.15 g) decreased the selectivity of IPA due to the formation of benzaldehyde and benzoic acid, which demonstrated the fact that, increment in active sites (i.e. Ag), aromatic C_{sp2}- C_{sp3} bond breakage is facilitated. Maintaining all the optimum conditions, when the reaction was allowed to run for hours, we didnot notice any marked effect in the yield of IPA after 10h, probably due to the decomposition of H_2O_2 present in the reaction medium (Fig. S23, ESI†).

To investigate the possible catalytic activity of Ag-species in the oxidation of *m*-xylene, various commercial Ag-compounds were employed separately as catalysts (Entry 2-6, Table 1). Experimental results showed that no conversion of *m*-xylene, excluding the catalytic contribution of the free Ag^+ species to the C–H bond activation. Moreover, commercial WO_3 and even Ag-W catalyst prepared in the impregnation process (AgW^{imp}, Entry 8, Table 1) catalyst failed to produce IPA, indicating the fact that, neither WO_3 nor AgW^{imp} individually was enough for activating C–H bond of *m*-xylene; moreover, these catalysts bear large and non-uniform sizes, which limit the accessibility of the catalysts towards the reacting substrates.[11a] In contrast, our prepared catalyst possesses ultrasmall Ag, which are dispersed on WO_3 petals, which are efficiently oxidizes m-xylene to IPA.; probably, synergistic interaction between Ag and WO_3 in the catalyst plays vital role in this reaction. With our own interest, we employed our previously reported Ag-W nanorods catalyst (AgW^{NR}, Entry 9, Table 1), in the oxidation of *m*-xylene. In 10h, we noticed 55% conversion and 70% selectivity to IPA. Prolonged time (30h) furnished >99% conversion of *m*-xylene with75% selectivity to IPA was speculated. Ag-W catalyst with flower structure ($Ag\text{-}W^{urc}$) furnished IPA with ~96% yield in 10h (Entry 12, Table 1), which clearly indicates that this catalyst exhibits much higher catalytic activity (with TON = 503) than the corresponding rod-like form (with TON = 201), despite the fact that the same metal loading (1.3 %) was used and the BET surface areas for the two forms were comparable to each other (44 m^2/g). One possibility for this experimental finding is that, a higher dispersion of Ag (ultra small) anchored on the WO_3 support. Furthermore, HRTEM image (Fig S18, ESI) revealed the fact that two nanoparticles fused to form petals that comprises flower-like structure. This zone (interface junction) remains highly strained due to different orientation of the two different nanoparticles.[8,22]As a result, the Ag nanoparticles anchored on the WO_3 support remain in highly strained form. Based on this hypothesis, we came out of this inference that, Ag nanoparticles anchored on petals of flower-like structure are much more reactive than that on rods-like structures. This phenomenon is indicative of the remarkable activity dependence on the morphology of the Ag-W catalyst. It was also noticed that, higher loading of Ag decreased the yield of IPA, probably due to the fact that loading of Ag lead to the formation of Ag-agglomerates (as confirmed from TEM diagram, Fig S19, ESI†), that decreased the active metal dispersion and catalyst-efficacy. Furthermore, leaching test was performed, which ascertained that the catalyst can be reused several times (4 recycles). We observed that the catalyst showed negligible change in its activity (Table 1, entry 7 and Fig. S24, ESI†), confirming the true heterogeneity of the catalyst. Moreover, we also used (2,2,6,6-Tetramethyl-piperidin-1-yl)oxyl (TEMPO) as radical scavanger (10% by weight wrt *m*-xylene) while conducting the experiment maintaining its all optimum conditions. A drastic change in the conversion of *m*-xylene was noticed (Entry 14, Table 1), indicating the fact that the reaction follows radical-path way.

Table 1 Oxidation reaction of *m*-xylene over Ag-W flower-like Catalyst[a]

Entry	Catalyst	C_B[b] (%)	S_P[c(%)]				Y_A[d] (%)	TON[e]
			IPA	3-CBA	MTA	Others		
1	No catalyst	-	-	-	-	-		-
2	$AgNO_3$	-	-	-	-	-		-
3	AgCl	-	-	-	-	-		-
4	$AgNO_2$	-	-	-	-	-		-
5	Ag	-	-	-	-	-		-
6	Ag_2O	-	-	-	-	-		-
7	WO_3	-	-	-	-	-		-
8	$Ag\text{-}W^{imp}$	2.5	-	-	5	95	-	-
9	$Ag\text{-}W^{NR}$	55	70	25	3	2	38.5	201
10[f]	$Ag\text{-}W^{flw}$	>99	97	2	1	0	96	503
11[g]	$Ag\text{-}W^{flw}$	97	96	2	1.5	0.5	93.1	488
12[h]	$Ag\text{-}W^{flw}$	>99	87	6	4	3	86.1	122
13[i]	$Ag\text{-}W^{flw}$	>99	70	10	8	12	69.3	41
14[j]	$Ag\text{-}W^{flw}$	2.8	-	-	-	>99	-	-

[a] Reaction Condition: *m*-xylene =1g; solvent = DMSO; catalyst = 0.15g; m-xylene : H_2O_2 mole ratio =1: 6; time= 10 h; temperature= 70 °C. [b] C_B = Conversion of m-xylene; [c]S_P = Selectivity of products; [d] Y_A = Yield of IPA. [e] TON= turnover number calculated by moles of IPA formed/ one mol of Ag in the catalyst present as supported Ag (0). [f] Fresh and [g] spent (after 4 reuse) Ag-W flower-like catalyst (1.3% Ag loading). [h] 4.8% and [i] 11.5% Ag loading. [j] Using TEMPO (radical scavenger).

Acknowledgements
SSA and SG thank CSIR and UGC, New Delhi, India, for their respective fellowships. R.B. thanks CSIR, New Delhi, for financial support in the form of the 12 FYP Project (CSC- 0125, CSC- 0117). The Director, CSIR-IIP is acknowledged for his help and encouragement. The authors thank ASD Division, IIP for the analytical services. We gratefully acknowledge Ms. Nishita Lucas,

CSIR-NCL, Pune (India), for performing Raman spectroscopy analyses.

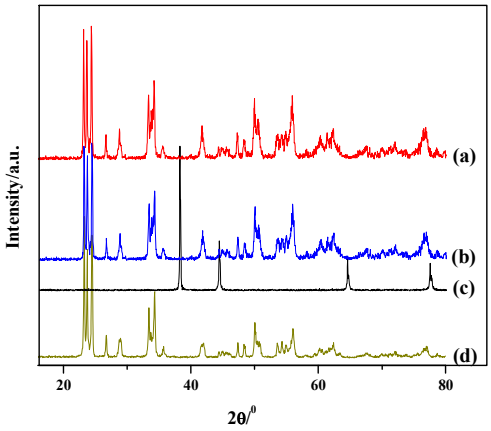

Fig. 1 XRD diffractogram of (a) fresh catalyst, (b) spent catalyst (after 4 recycles), commercial (c) Ag and (d) WO_3.

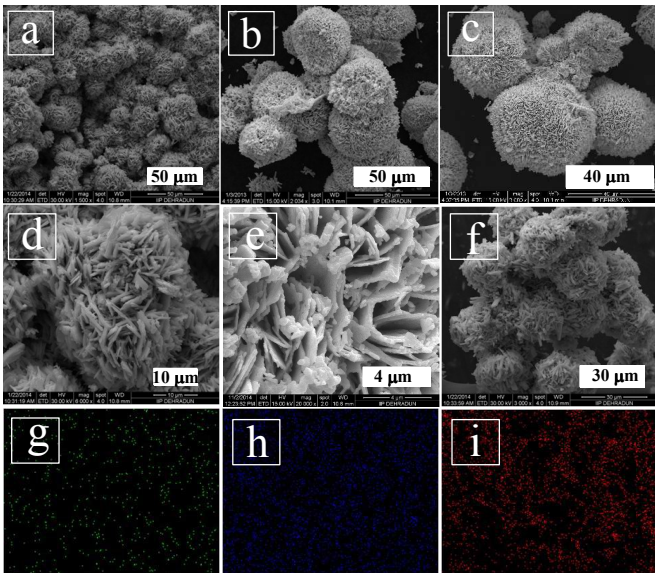

Fig. 2 SEM images of (a-d) fresh catalyst at ascending magnification and that of (e) spent catalyst and elemental mapping (based on Fig. 3e) of (g) Ag, (h) W and (i) O in the catalyst.

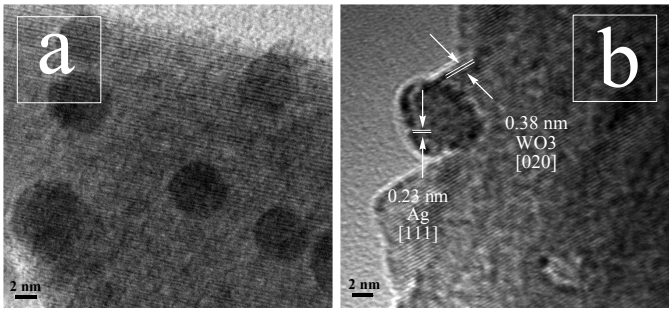

Fig. 3 (a-b) TEM images of the catalyst at ascending magnification.

Conclusions

In summary, 3D flower-like hierarchical Ag-WO_3 microspheres with a 30-50 µm diameter can be prepared by the surfactant CTAB assisted method. The catalyst displayed excellent catalytic performance in the sustainable oxidation of *m*-xylene to isophthalic acid with H_2O_2 as oxidant, achieving high efficiency in terms of activity, selectivity and stability. The attractive features of the catalyst are very promising, as it may serve as an avenue to meet the urgent demand of isophthalic acid and the process might be potential alternative to the existing Amoco-process.

Notes and references

[a] Catalytic Conversion & Processes Division, CSIR-Indian Institute of Petroleum, Dehradun, India, E-mail: raja@iip.res.in.

† Electronic Supplementary Information (ESI) available: Detailed experimental procedure, characterization techniques, effects of various reaction parameters etc. See DOI: 10.1039/c000000x/

1 (a) C. Burda, X. B. Chen, R. Narayanan and M. A. El-Sayed, *Chem. Rev.,* 2005, **105**, 1025;
2 M. S. Mo, J. C. Yu, L. Z. Zhang and S. K. A. Li, *Adv. Mater.,* 2005, **17**, 756.
3 L. S. Zhong, J. S. Hu, H. P. Liang, A. M. Cao, W. G. Song and L. J. Wan, *Adv. Mater.,* 2006, **18**, 242.
4 C. B. Cao, Z. Chen, X. Q. An and H. S. Zhu, *J. Phys. Chem. C,* 2008, **112**, 95.
5 X. H. Li, D. H. Zhang and J. S. Chen, *J. Am. Chem. Soc*., 2006, **128**, 8328.
6 A. M. Cao, J. S. Hu, H. P. Liang and L. J. Wan, *Angew. Chem.,* 2005, **44**, 4391.
7 L. Y. Chen, D. Zhang and W. Z. Wang, *J. Phys. Chem. C.,* 2008, **112**, 4117.
8 W. Hao, S. Chen, Y. Cai, L. Zhang, Z. Li and S. Zhang, *J. Mater Chem. A,* 2014, **2**, 13801.
9 (a) Z. P. Zhang, X. Q. Shao, H. D. Yu, Y. B. Wang and M. Y. Han, *Chem. Mater.,* 2005, **17**, 332.
10 S. S. Acharyya, S. Ghosh and R. Bal, *ACS Appl. Mater. Interfaces,* 2014, **6**, 14451.
11 (a) S. Ghosh, **S. S.** Acharyya, S. Adak, L.N. S. Konathala, T. Sasaki and R. Bal, *Green Chem.,* 2014, **16**, 2826; (b) S. Ghosh, S. S. Acharyya, R. Tiwari, B. Sarkar, R. K. Singha, C. Pendem, T. Sasaki and R. Bal, *ACS Catal.,* 2014, **4**, 2169; (c) S. Ghosh, S. S. Acharyya and R. Bal, *J. Mater. Chem. A*, 2014, **2**, 15726; (d) S. Ghosh, S. S. Acharyya, T. Sasaki and R. Bal, *Green Chem*., 2015 **DOI: 10.1039/C4GC02123A.**
12 R. A. F. Toma´s, J. C. M. Bordado and J. F. P. Gomes, *Chem. Rev.,* 2013, **113**, 7421.
13 Y. Ishii, Y. Yoshino and Y. Hayashi, *J. Org. Chem.,* 1997, **62,** 6810.
14 B. Saha, N. Koshino and J. H. Espenson, *J. Phys. Chem. A,* 2004, **108**, 425.
15 B. B. Wentzel, M. P. J. Donners, P. L. Alsters, M. C. Feiters and R. J. M. Nolte, *Tetrahedron,* 2000, **56**, 7797.
16 (a) H. Lv, S. Wu, N. Liu, X. Long and W. Yuan, *Chem. Eng. J.,* 2011, **172**, 1045; (b) X. Long, Z. Wang, S. Wu, S. Wu, H. Lv, W. Yuan, *J. Ind. Eng. Chem.,* 2014, **20**, 100.
17 H. He, B. J. Pei and A. W. M. Lee, *Green Chem.,* 2009, **11**, 1857.
18 K. Deori, D. Gupta, B. Saha and S. Deka, *ACS Catal.*, 2014, **4**, 3169.
19 X. L. Li, J. F. Liu and Y. D. Li, *Inorg. Chem.,* 2003, **42**, 921.
20 O. Yayapao, T. Thongtem, A. Phuruangrat and S. Thongtem, *J. Alloys Compd.,* 2011, **509**, 2294.
21 C. L. Kuo and K. C. Hwang, *Langmuir*, 2012, **28**, 3722.